

Reduced-Order Models for Thermal Radiative Transfer Based on POD-Galerkin Method and Low-Order Quasidiffusion Equations

Joseph M. Coale^{a,b}, Dmitriy Y. Anistratov^{a,c}

^a*Department of Nuclear Engineering North Carolina State University Raleigh, NC*

^b*jmcoale@ncsu.edu*

^c*anistratov@ncsu.edu*

Abstract

This paper presents a new technique for developing reduced-order models (ROMs) for nonlinear radiative transfer problems in high-energy density physics. The proper orthogonal decomposition (POD) of photon intensities is applied to obtain global basis functions for the Galerkin projection (POD-Galerkin) of the time-dependent multigroup Boltzmann transport equation (BTE) for photons. The POD-Galerkin solution of the BTE is used to determine the quasidiffusion (Eddington) factors that yield closures for the nonlinear system of (i) multilevel low-order quasidiffusion (VEF) equations and (ii) material energy balance equation. Numerical results are presented to demonstrate accuracy of the ROMs obtained with different low-rank approximations of intensities.

Keywords: high-energy density physics, thermal radiative transfer, Boltzmann equation, reduced-order modeling, nonlinear PDEs, proper orthogonal decomposition, Galerkin projection, multilevel methods

1. Introduction

In this paper, we develop reduced order models (ROMs) for the basic thermal radiative transfer (TRT) problem that neglects material motion, scattering and heat conduction. Problems in 1D slab geometry are considered. The TRT problem is defined by the time-dependent multigroup Boltzmann transport equation (BTE) given by

$$\frac{1}{c} \frac{\partial I_g}{\partial t}(x, \mu, t) + \mu \frac{\partial I_g}{\partial x}(x, \mu, t) + \kappa_g(T) I_g(x, \mu, t) = 2\pi \kappa_g(T) B_g(T) \quad (1)$$

$$x \in [0, X], \quad \mu \in [-1, 1], \quad g = 1, \dots, N_g, \quad t \in [0, t_{end}],$$

$$I_g|_{x=0}^{\mu>0} = I_g^{\text{in}+}, \quad I_g|_{x=X}^{\mu<0} = I_g^{\text{in}-}, \quad I_g|_{t=0} = I_g^0, \quad (2)$$

and the material energy balance (MEB) equation

$$\frac{\partial \varepsilon(T)}{\partial t} = \sum_{g=1}^{N_g} \kappa_g(T) \left(\int_{-1}^1 I_g(x, \mu, t) d\mu - 4\pi B_g(T) \right), \quad T|_{t=0} = T_0. \quad (3)$$

Here I_g is the group specific photon intensity; x is the spatial position; μ is the direction cosine of particle motion; g is the index of photon frequency group; N_g is the number of frequency groups; t is time; κ_g is the group material opacity; T is the material temperature; ε is the material energy density and B_g is the group Planck black-body distribution function. The BTE describes propagation and absorption of photons in matter, and emission of photons with the black-body spectrum. The MEB equation models change in material energy as the result of absorption and emission of photons.

Particle transport problems have high dimensionality; Discretization of the BTE in the phase space and time results in a problem with a very large number of degrees of freedom (DoF). This has stimulated active research on the development of ROMs for the BTE and its related class of problems [1, 2, 3, 4, 5]. In this study, the new ROMs for TRT problems (1)-(3) are based on the proper orthogonal decomposition (POD) and projection approach [6, 7, 8]. The POD creates an optimal basis to represent dynamics of a system based on a set of collected data [9]. Specifically, the reduced basis for a Galerkin expansion of intensities over the phase space is generated by the POD of a collection of vectors of numerical transport solutions over time intervals of the TRT problem. The BTE is projected onto this basis. The POD-Galerkin projected BTE can be viewed as a discretization scheme based on a set of problem-specific global basis functions. The projected BTE is then coupled with the multilevel nonlinear system of governing moment equations consisting of (i) low-order quasidiffusion (aka VEF) equations for the group and total radiation energy densities and fluxes and (ii) MEB equation. The moment equations are derived by a nonlinear projection of the BTE (Eq. (1)) using exact closures by means of quasidiffusion (Eddington) factors. The POD-Galerkin expansion of intensities is used to compute the quasidiffusion (QD) factors.

The remainder of the paper is organized as follows. In Sec. 2.1 POD-Galerkin projection of the BTE is formulated. In Sec. 2.2 the ROM based on multilevel low-order QD equations is described. Numerical results are presented in Sec. 3. We conclude with a brief discussion in Sec. 4.

2. Reduced-Order Model for TRT

2.1. POD-Galerkin Projection of BTE

To discretize the BTE (1) we apply (i) the method of discrete ordinates (MDO) for the angular variable, (ii) the backward Euler (BE) scheme for time integration, and (iii) the simple corner-balance (SCB) method for approximation in space [10] to obtain

$$\frac{1}{c\Delta t^n}(\mathbf{I}^n - \mathbf{I}^{n-1}) + \mathcal{L}_h\mathbf{I}^n + \mathcal{K}_h^n(T)\mathbf{I}^n = \mathbf{Q}^n(T), \quad (4)$$

where n is the time step index, $\mathbf{I}^n = ((\mathbf{I}_1^n)^\top \dots (\mathbf{I}_{N_g}^n)^\top)^\top \in \mathbb{R}^D$ is the solution vector at $t = t^n$, $\mathbf{I}_g^n \in \mathbb{R}^{2N_x N_\mu}$ is the vector of group intensities, $D = 2N_x N_\mu N_g$ is the number of DoF in the phase space, N_x is the number of spatial mesh cells, N_μ is the number of discrete angular directions, \mathcal{L}_h and \mathcal{K}_h are the discrete operators that define approximation by the

MDO and the SCB scheme, $\mathbf{Q}^n(T)$ is the vector of the right-hand side, Δt^n is the n^{th} time step.

The numerical solution of the discretized BTE (4) on a given phase-space grid is used to form a database matrix $\mathbf{A} = [\mathbf{I}^1, \dots, \mathbf{I}^{N_t}] \in \mathbb{R}^{D \times N_t}$ of the solution snapshots computed over N_t time steps. The database \mathbf{A} is used to form a POD basis $\{\mathbf{u}_\ell\}_{\ell=1}^r$ with $r \ll D$ that gives an optimal approximation of \mathbf{A} and solves the following optimization problem [11]:

$$\min_{\mathbf{u}_1, \dots, \mathbf{u}_r} \sum_{n=1}^{N_t} \Delta t^n \left\| \mathbf{I}^n - \sum_{\ell=1}^r \langle \mathbf{I}^n, \mathbf{u}_\ell \rangle_W \mathbf{u}_\ell \right\|_W^2, \quad (5)$$

where the norm $\|\cdot\|_W^2$ is defined by the spatial and angular discretization of the BTE. The weighted inner product specific to the SCB and MDO discretization is given by $\langle \mathbf{u}_\ell, \mathbf{u}_{\ell'} \rangle_W = \mathbf{u}_\ell^\top \mathbf{W} \mathbf{u}_{\ell'}$ with

$$\mathbf{W} = \bigoplus_{g=1}^{N_g} \bigoplus_{m=1}^{N_\mu} w_m \hat{\mathbf{W}}^x, \quad \mathbf{W} \in \mathbb{R}^{D \times D}. \quad (6)$$

Here w_m are the angular quadrature weights, and $\hat{\mathbf{W}}^x = \bigoplus_{i=1}^{N_x} \frac{\Delta x_i}{2} \mathbb{I}$, where $\mathbb{I} \in \mathbb{R}^{2 \times 2}$ is the identity matrix. We form the weighted data matrix

$$\hat{\mathbf{A}} = \mathbf{W}^{1/2} \mathbf{A} \mathbf{D}^{1/2} \quad \text{with} \quad \mathbf{D} = \text{diag}(\Delta t^1, \dots, \Delta t^{N_t}) \quad (7)$$

and find its singular value decomposition (SVD) to get

$$\hat{\mathbf{A}} = \hat{\mathbf{U}} \hat{\mathbf{\Sigma}} \hat{\mathbf{V}}^\top, \quad (8)$$

where $\hat{\mathbf{U}} = [\hat{\mathbf{u}}_1, \dots, \hat{\mathbf{u}}_d] \in \mathbb{R}^{D \times d}$ holds the left singular vectors of $\hat{\mathbf{A}}$ in its columns, $\hat{\mathbf{V}} \in \mathbb{R}^{N_t \times d}$ is the matrix of the right singular vectors, $\hat{\mathbf{\Sigma}} = \text{diag}(\sigma_1, \dots, \sigma_d) \in \mathbb{R}^{d \times d}$ is the matrix of singular values, $d = \min(D, N_t)$ is the rank of $\hat{\mathbf{A}}$. The POD basis $\mathbf{U} = [\mathbf{u}_1, \dots, \mathbf{u}_d] \in \mathbb{R}^{D \times d}$ satisfying Eq. (5) is given by

$$\mathbf{U} = \mathbf{W}^{-1/2} \hat{\mathbf{U}}. \quad (9)$$

We now formulate Galerkin ansatz expanding the intensities in the POD basis (9) [8, 11]

$$\mathbf{I}_r^u(t^n) = \sum_{\ell=1}^r \lambda_\ell^n \mathbf{u}_\ell, \quad r \leq d. \quad (10)$$

The discretized transport equation (4) is projected onto the POD basis to derive the POD-Galerkin (POD-G) projected BTE ($\ell = 1, \dots, r$) given by

$$\frac{1}{c \Delta t^n} (\lambda_\ell^n - \lambda_\ell^{n-1}) + \sum_{\ell'=1}^r \lambda_{\ell'}^n \langle \mathbf{u}_\ell, \mathcal{L}_h \mathbf{u}_{\ell'} \rangle_W + \sum_{\ell'=1}^r \lambda_{\ell'}^n \langle \mathbf{u}_\ell, \mathcal{K}_h^n(T) \mathbf{u}_{\ell'} \rangle_W = \langle \mathbf{u}_\ell, \mathbf{Q}^n(T) \rangle_W, \quad (11)$$

where it is taken into account that $\langle \mathbf{u}_{\ell'}, \mathbf{u}_\ell \rangle_W = \delta_{\ell, \ell'}$. The POD basis is a global one. This yields a non-sparse system of equations for the coefficients λ_ℓ^n at $t = t^n$. However, it will be shown below that the ROMs based on the POD-G projected BTE (11) are accurate for $r \ll D$.

2.2. ROM Based on Multilevel Low-Order QD Equations

The system of equations of the multilevel QD (MLQD) method for the TRT problem (1)-(3) is derived by a nonlinear projection in angular and frequency (photon energy) spaces. It is defined by the following low-order equations [12, 13, 14]:

1. The multigroup low-order QD (LOQD) equations for the angular moments given by

$$\frac{\partial E_g}{\partial t} + \frac{\partial F_g}{\partial x} + c\kappa_g(T)E_g = 4\pi\kappa_g(T)B_g(T), \quad (12a)$$

$$\frac{1}{c} \frac{\partial F_g}{\partial t} + c \frac{\partial}{\partial x} (f_g[I]E_g) + \kappa_g(T)F_g = 0, \quad (12b)$$

where $E_g = \frac{1}{c} \int_{-1}^1 I_g d\mu$ is the group radiation energy density, $F_g = \int_{-1}^1 \mu I_g d\mu$ is the group radiation flux, and

$$f_g[I] = \int_{-1}^1 \mu^2 I_g d\mu / \int_{-1}^1 I_g d\mu \quad (13)$$

is the group QD (Eddington) factor that provides closure of the BTE and multigroup LOQD equations. This closure is exact when f_g is defined by the solution of the BTE (1) according to the QD (VEF) method [12, 15].

2. The effective grey LOQD equations for the total radiation energy density $E = \sum_{g=1}^{N_g} E_g$ and the total flux $F = \sum_{g=1}^{N_g} F_g$ are given by

$$\frac{\partial E}{\partial t} + \frac{\partial F}{\partial x} + c\bar{\kappa}_E E = c\bar{\kappa}_B a_R T^4, \quad (14a)$$

$$\frac{1}{c} \frac{\partial F}{\partial t} + c \frac{\partial (\bar{f}[I]E)}{\partial x} + \bar{\kappa}_R F + \bar{\eta} E = 0, \quad (14b)$$

where the grey coefficients are

$$\bar{\kappa}_E = \frac{\sum_{g=1}^{N_g} \kappa_g E_g}{\sum_{g=1}^{N_g} E_g}, \quad \bar{\kappa}_B = \frac{\sum_{g=1}^{N_g} \kappa_g B_g}{\sum_{g=1}^{N_g} B_g}, \quad \bar{\kappa}_R = \frac{\sum_{g=1}^{N_g} \kappa_g |F_g|}{\sum_{g=1}^{N_g} |F_g|},$$

$$\bar{f} = \frac{\sum_{g=1}^{N_g} f_g E_g}{\sum_{g=1}^{N_g} E_g}, \quad \bar{\eta} = \frac{\sum_{g=1}^{N_g} (\kappa_g - \bar{\kappa}_R) F_g}{\sum_{g=1}^{N_g} E_g}.$$

The grey LOQD equations are coupled with the MEB equation that is cast in grey form for the total energy density

$$\frac{\partial \varepsilon(T)}{\partial t} = c(\bar{\kappa}_E E - \bar{\kappa}_B a_R T^4). \quad (15)$$

The new ROM for TRT combines the POD-G projected BTE with nonlinear projection in angular variable and photon energy via the hierarchy of low-order QD equations for moments of the intensity. It is defined by the following set of equations:

- the POD-G projected BTE (Eq. (11)) the solution of which gives compressed representation of the intensities in the phase space,
- the multigroup LOQD equations (Eq. (12)), where the QD factors are defined by the POD-G expansion of intensities of rank r and hence

$$f_g^u = f_g [\mathbf{I}_r^u], \quad (16)$$

- the effective grey LOQD equations (Eq. (14)) and the MEB equation in the grey form (Eq. (15)).

The QD factor f_g^u defines an approximate closure for the group LOQD equations providing further data compression of intensities and the next level of reduction of dimensionality for the TRT problem. Hereafter we refer to this ROM as the QD-PODG model, whose iterative algorithm for solving TRT problems is outlined in Algorithm 1. Temporal discretization of the LOQD and MEB equations (Eqs. (12), (14), and (15)) is based on the BE time integration method. The multigroup LOQD equations are discretized in space by means of a second-order finite volume (FV) method [16]. The spatial discretization of the grey LOQD equations is algebraically consistent with the discretized multigroup LOQD equations.

The coefficients of the POD-G projected BTE explicitly depend on T through group opacities and the Planckian emission term. This makes Eq. (11) an integral part of the nonlinear multilevel system of LOQD equations by means of which they are coupled to the MEB equation. This feature allows these equations to be used in the development of parameterized ROMs for TRT. One can generate the POD-G basis $\{\mathbf{u}_\ell\}_{\ell=1}^r$ for a base case TRT problem and use the QD-PODG model with this basis to solve TRT problems with different parameters, for example, a perturbed spectrum of incoming radiation.

3. Numerical Results

To analyze the accuracy of the QD-PODG model, we use the problem based on the well-known Fleck-Cummings (F-C) test [17]. A 1D slab of one material is defined as 6 cm thick ($X = 6$). The material spectral opacity is given by $\kappa_\nu = \frac{27}{(h\nu)^3} (1 - e^{-\frac{h\nu}{kT}})$. The left boundary has incoming radiation with black-body spectrum B_ν at temperature $kT_{in} = 1$ keV and the right boundary is vacuum. The initial temperature of the slab is $kT_0 = 1$ eV and the initial radiation distribution is given by the black-body spectrum at T_0 . The material energy density is a linear function of temperature $\varepsilon = c_\nu T$, where $c_\nu = 0.5917 a_R T_{in}^3$. The time interval of the problem is $0 \leq t \leq 6$ ns. A uniform time step is used $\Delta t = 2 \times 10^{-2}$ ns and hence there are 300 time steps ($N_t = 300$). The spatial mesh consists of a uniform $N_x = 60$ cells with width $\Delta x = 0.1$ cm. The angular mesh has 8 discrete directions ($N_\mu = 8$). The double S_4 Gauss-Legendre quadrature set is used. We define $N_g = 17$ energy groups. The parameters of convergence criteria for temperature and energy density are $\epsilon_T = \epsilon_E = 10^{-12}$, respectively.

The full-order model (FOM) for this TRT problem is formulated as the MLQD method where the BTE and low-order QD equations are discretized as described above on the given

```

while  $t_n \leq t^{\text{end}}$  do
   $n = n + 1$ 
   $T^{(0)} = T^{n-1}$ 
  while  $\|T^{(k)} - T^{(k-1)}\| > \epsilon_T \|T^{(k)}\|$ ,  $\|E^{(k)} - E^{(k-1)}\| > \epsilon_E \|E^{(k)}\|$  do
     $k = k + 1$ 
    Update  $\varkappa_g, B_g$  using  $T^{(k-1)}$ 
    Solve POD-G projected BTE (Eq. (11)) given  $\{\mathbf{u}_\ell\}_{\ell=1}^r$ ,  $T^{(k-1)}$  to compute
       $\{\lambda_\ell^{(k)}\}_{\ell=1}^r$ 
    Compute  $\mathbf{I}_r^{u(k)} = \sum_{\ell=1}^r \lambda_\ell^{(k)} \mathbf{u}_\ell$ 
    Compute  $f_g^{u(k)} = f_g[\mathbf{I}_r^{u(k)}]$ 
    while  $\|T^{(k,s)} - T^{(k,s-1)}\| > \epsilon_T \|T^{(k,s)}\|$ ,  $\|E^{(k,s)} - E^{(k,s-1)}\| > \epsilon_E \|E^{(k,s)}\|$  do
       $s = s + 1$ 
      Update  $\varkappa_g, B_g$  using  $T^{(k,s-1)}$ 
      Solve Eqs. (12) given  $f_g^{u(k)}$  to compute  $E_g^{(k,s)}, F_g^{(k,s)}$ 
      Compute grey coefficients  $\bar{\varkappa}_E^{(k,s)}, \bar{\varkappa}_B^{(k,s)}, \bar{\varkappa}_R^{(k,s)}, \bar{f}^{(k,s)}, \bar{\eta}^{(k,s)}$ 
      Solve Eqs. (14) and (15) to compute  $E^{(k,s)}, F^{(k,s)}, T^{(k,s)}$ 
    end
     $T^{(k)} \leftarrow T^{(k,s)}$ 
  end
   $T^n \leftarrow T^{(k)}$ ,  $\lambda_\ell^n \leftarrow \lambda_\ell^{(k)}$ 
end

```

Algorithm 1: The algorithm of the QD-PODG model for solving TRT problems

grid in phase space and time. The number of DoF of \mathbf{I}^n at each instant of time t^n is $D = 1.632 \times 10^4$. The number of DoF in the phase space and time for this FOM is equal to $DN_t = 4.896 \times 10^6$. The solution to the F-C test evolves in three distinct temporal stages: (i) rapid wave formation, (ii) wave propagation, and (iii) slow continual heating of the domain to steady state. A separate database is constructed by the FOM for each of these stages, whose temporal ranges are the following: $t \in [0, 0.3 \text{ ns}]$ for $i = 1$, $t \in (0.3, 1.2 \text{ ns}]$ for $i = 2$, $t \in (1.2, 6 \text{ ns}]$ for $i = 3$.

The resulting database matrices that hold the set of discrete intensities for each of the three stages of the F-C test we denote by $\mathbf{A}_i \in \mathbb{R}^{D \times N_{t,i}}$, $i = 1, 2, 3$. The columns of each database are snapshots of the solution at $N_{t,1}, N_{t,2}, N_{t,3}$ instants of time, respectively, ordered chronologically. The full ranks d_i of \mathbf{A}_i are equal to $d_1 = N_{t,1} = 15$, $d_2 = N_{t,2} = 45$, $d_3 = N_{t,3} = 240$ respectively. The singular values (σ_ℓ) of each of the three databases are depicted in Figure 1. The first database shows a slow rate of decrease in magnitude of its singular values over the entire range, whereas the singular values of the other two databases first experience rapid decrease followed by a plateau where the change in their magnitudes slows significantly. From the matrices \mathbf{A}_i , POD bases $\{\mathbf{u}_{i,\ell}\}_{\ell=1}^{r_i}$, $i = 1, 2, 3$ are calculated for each of these time intervals.

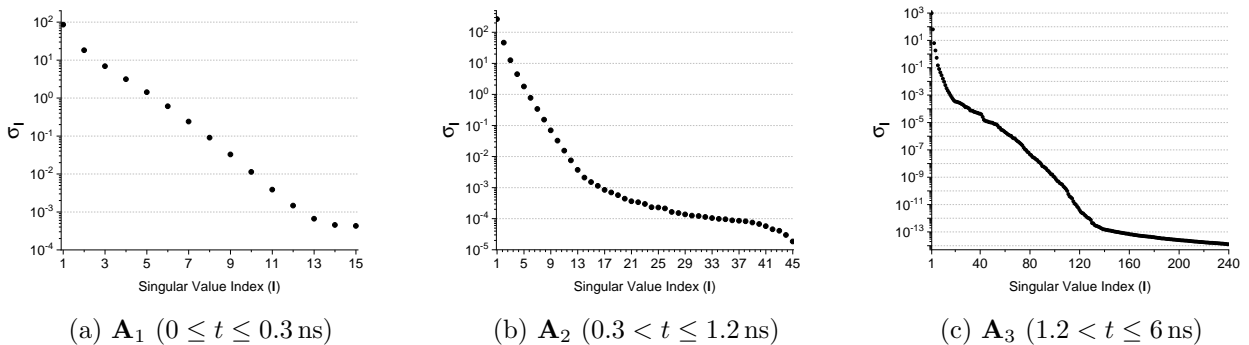


Figure 1: Singular values of the database matrices of intensities over three time subintervals of the problem

We now solve the F-C test with the QD-PODG model by expanding I with each of our three POD bases based on the time frames they were generated for (e.g. we expand with $\{\mathbf{u}_{1,\ell}\}_{\ell=1}^{r_1}$ while $0 \leq t \leq 0.3$ ns). The ranks (r_1, r_2, r_3) of the expansion (10) are determined as the values that satisfy the following criterion [6]

$$\left(\sum_{\ell=r_i+1}^{d_i} \sigma_\ell^2 / \sum_{\ell=1}^{d_i} \sigma_\ell^2 \right)^{\frac{1}{2}} < \varepsilon, \quad \text{for } A_i, i = 1, 2, 3, \quad (17)$$

given some desired ε . The ranks found for $\varepsilon \in [10^{-5}, 10^{-16}]$ are shown in Figure 2. The POD bases for \mathbf{A}_1 and \mathbf{A}_2 reach full rank ($r_1 = 15$, $r_2 = 45$) at $\varepsilon = 10^{-6}$ and $\varepsilon = 10^{-8}$, respectively. Full-rank is not found for the basis of \mathbf{A}_3 ($r_3 = 240$) until $\varepsilon = 10^{-16}$. This behavior is expected since compared to \mathbf{A}_3 , the full ranks of \mathbf{A}_1 and \mathbf{A}_2 are relatively small. The singular values of both \mathbf{A}_1 and \mathbf{A}_2 also occupy a smaller range than for \mathbf{A}_3 . Another notable behavior is that $r_3 < r_2$ for $\varepsilon < 10^{-8}$, indicating that the solution contained in the time range over which \mathbf{A}_2 was generated is the most difficult to represent with few POD modes. This is to be expected given that \mathbf{A}_2 accounts for the solution during propagation of the radiation wave from the left boundary to the right, which is known to be a difficult phenomena for the POD to represent with low rank [18, 19]. Let us note here that the rank of expansion for each timeframe in the F-C test is exactly the size of the linear system that solves for the coefficients λ_ℓ (Eq. (11)). This means that when using $\varepsilon = 10^{-5}$ for instance, the largest linear system to solve in place of the BTE is a dense $r \times r$ system with $r = 14$, which is of significantly lower dimensionality than the original BTE ($r = 14 \ll D = 1.632 \times 10^4$).

The errors of the QD-PODG model relative to the FOM solution on the F-C test in the 2-norm are displayed in Figure 3 for material temperature and radiation energy density vs. time. Each unique curve shows the relative error of the ROM solution for a specific value of ε , ranging from 10^{-5} to 10^{-16} . Note that we use the FOM solution as the reference to compute errors against, to determine how the ROM solution converges to its training data. The MLQD discrete solution will converge to the multigroup TRT solution in the limit $N_x, N_\mu, N_t \rightarrow \infty$ and so we can postulate that if the solution of the QD-PODG model

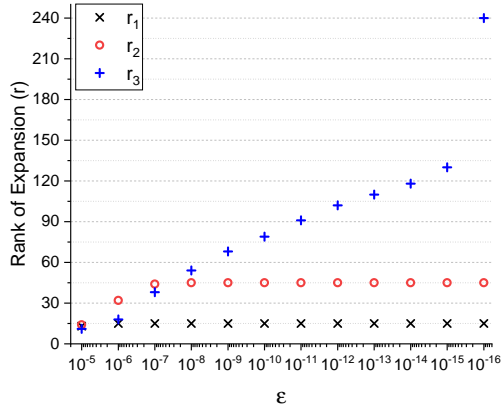
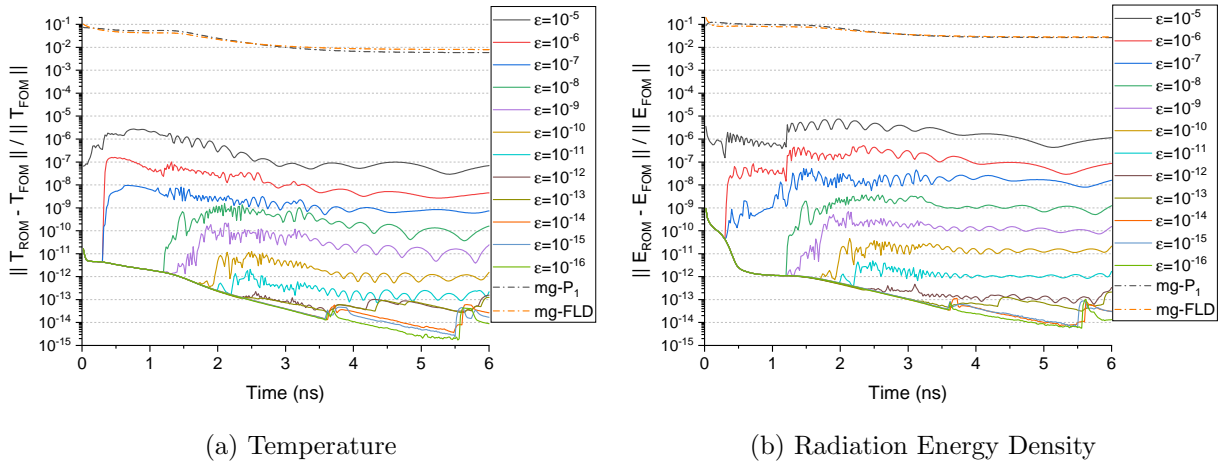


Figure 2: Rank of expansion for each database corresponding to different ε



(a) Temperature

(b) Radiation Energy Density

Figure 3: Relative errors of the QD-PODG model $mg-P_1$ and $mgFLD$ ROMs compared to the FOM solution in the 2-norm vs. time

converges to the discrete FOM solution then it will too converge to the continuous solution given a database generated on a fine-enough grid.

Figure 3 shows that as ε decreases, the relative error of the QD-PODG model trends downward as well. Upon inspection, one can see that the ROM with $\varepsilon = 10^{-6}, 10^{-7}$ is exceptionally accurate for $t \leq 0.3$ ns. This comes from the full-rank basis representation of \mathbf{A}_1 that occurs for all $\varepsilon < 10^{-5}$, as was shown in Figure 2. Similarly, the high accuracy for $t \leq 1.2$ while using $\varepsilon < 10^{-7}$ follows from the fact that the full-rank basis representation of \mathbf{A}_2 is used for $\varepsilon < 10^{-7}$. Considering overall accuracy, even with very low-rank ($\varepsilon = 10^{-5}$) the QD-PODG model maintains a relative error in both material temperature and radiation energy density below 10^{-5} . Figure 4 depicts the solution to the F-C test generated with the QD-PODG model, using the criterion from equation (17) as $\varepsilon = 10^{-5}$. This ROM can be compared to the relative errors in the 2-norm of the popular multigroup P_1 ($mg-P_1$) and

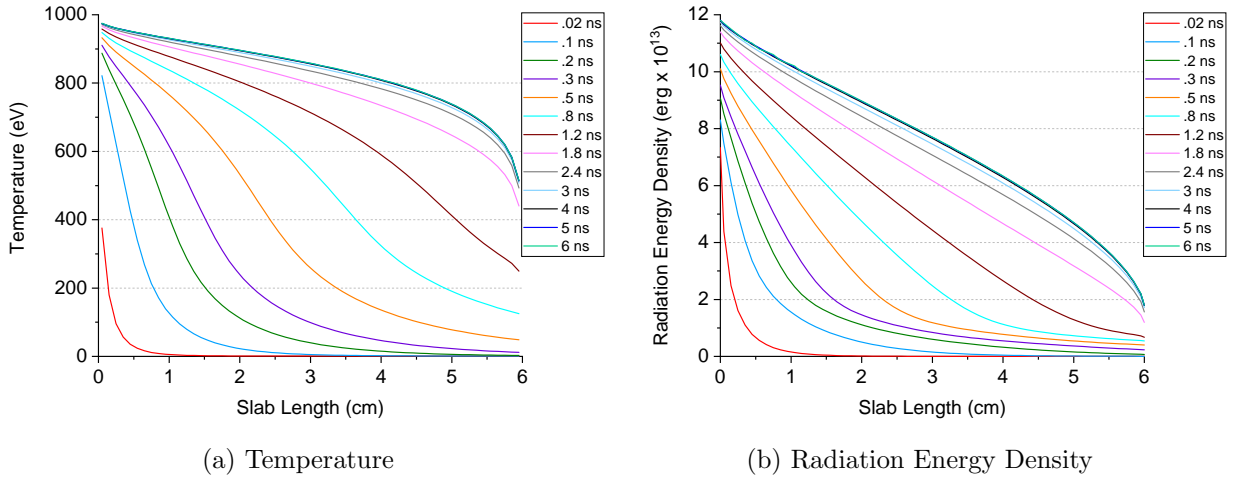


Figure 4: The solution to the F-C test on the given grid in phase space and time generated by the QD-PODG model with $\varepsilon = 10^{-5}$.

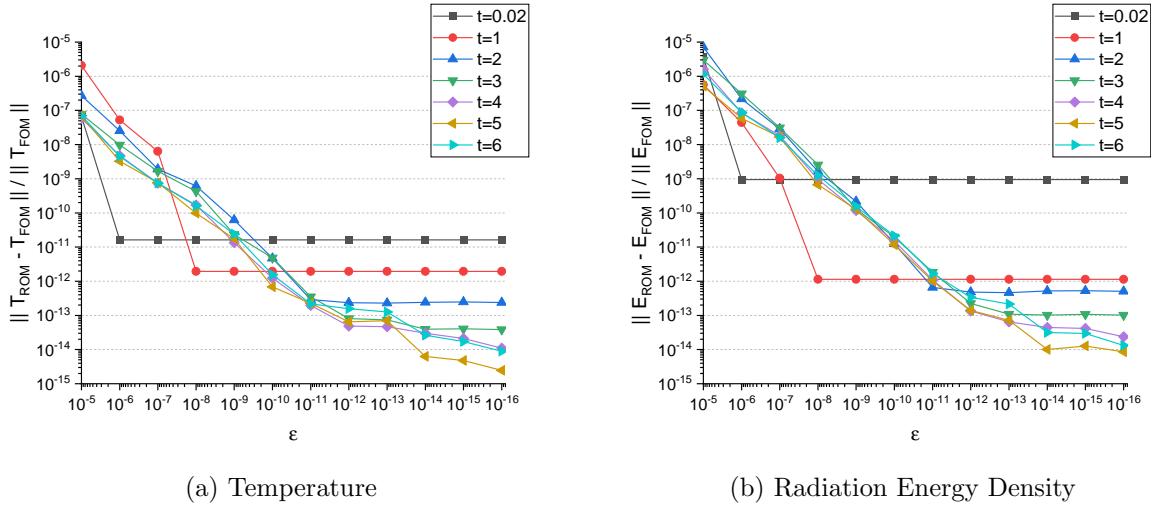


Figure 5: Relative errors of the QD-PODG model compared to the FOM solution in the 2-norm vs. ε

multigroup flux-limited diffusion (mg-FLD) ROMs [20] found for the same test problem, also shown in Figure 3. The results show that even with $\varepsilon = 10^{-5}$ the QD-PODG model yields a far more accurate solution than these other ROMs by roughly 3-4 orders of magnitude. Let us also take note that when using all POD modes ($\varepsilon = 10^{-16}$) the QD-PODG model converges to the FOM solution within the iterative convergence bounds with the exception of the radiation energy density while $t < 0.5$ ns. This comes from higher errors found at the radiation wavefront during formation, which is a difficult process to capture given how rapidly it progresses and can be prone to larger numerical errors than other parts of the solution.

Similarly to Figure 3, Figure 5 also displays the relative error in the solution of the F-C test obtained by the QD-PODG ROM compared to the FOM solution in the 2-norm, but

plotted in a unique format. In Figure 5 each curve corresponds to a specific instant of time, showing how the error of the QD-PODG model changes with respect to ε when time is held static. This plot clearly demonstrates the convergence behavior of the ROM solution as ε decreases to zero.

4. Conclusions

In this paper, we presented a new ROM for high-energy density TRT problems. The proposed methodology is based on the nonlinear projection approach and Galerkin projection combined with the POD. The developed ROM efficiently reduces dimensionality of TRT problems and was shown capable of producing solutions with various levels of fidelity. The accuracy varies based on the rank of the POD basis used to project the BTE, and the ROM solution converges to the FOM solution as this rank is increased. As such the developed ROMs enable the use of practical and efficient simulations by significantly reducing dimensionality of the problem while maintaining sufficient accuracy. The ROMs presented here also possess the capability for parameterization, which is an avenue the authors will be pursuing in the future.

The promising performance of the QD-PODG model motivates further research on this approach. An extension to 2D geometry is the next logical step. To make the method robust for such extensions, a desirable feature is to enforce positivity of the expanded intensities. Secondly, work must be done towards generation of enhanced POD for the problems at hand; one technique would be to use symmetry-reduction methods [18, 19] which are known to improve basis generation for traveling waves.

Acknowledgments

This research project is funded by the Department of Defense, Defense Threat Reduction Agency, grant number HDTRA1-18-1-0042. The content of the information does not necessarily reflect the position or the policy of the federal government, and no official endorsement should be inferred.

References

- [1] J. Coale, D. Anistratov, A reduced-order model for thermal radiative transfer problems based on multilevel quasidiffusion method, in: Int. Conf. on Mathematics and Computational Methods Applied to Nuclear Science and Engineering (M&C 2019), Portland, OR, August 25, 2019, pp. 278–287.
- [2] J. Coale, D. Y. Anistratov, Data-driven grey reduced-order model for thermal radiative transfer problems based on low-order quasidiffusion equations and proper orthogonal decomposition, Transaction of American Nuclear Society 121 (2019) 836–839.
- [3] P. A. Behne, J. C. Ragusa, J. E. Morel, Model order reduction for S_n radiation transport, in: Int. Conf. on Mathematics and Computational Methods Applied to Nuclear Science and Engineering (M&C 2019), Portland, OR, August 25, 2019, pp. 2481–2490.
- [4] Z. Peng, R. G. McClarren, M. Frank, A low-rank method for two-dimensional time-dependent radiation transport calculations, Journal of Computational Physics 421 (2020) 109735.

- [5] Y. Choi, P. Brown, B. Arrighi, R. Anderson, Space-time reduced order model for large-scale linear dynamical systems with application to boltzmann transport problems, *Journal of Computational Physics* 424 (2021) 109845.
- [6] L. Sirovich, Turbulence and the dynamics of coherent structures. parts i-iii, *Quarterly of Applied Mathematics* XLV (1987) 561–590.
- [7] G. Berkooz, P. Holmes, J. L. Lumley, The proper orthogonal decomposition in the analysis of turbulent flows, *Annual Review of Fluid Mechanics* 25 (1993) 539–575.
- [8] K. Kunisch, S. Volkwein, Galerkin proper orthogonal decomposition methods for a general equation in fluid dynamics, *SIAM J. Numer. Anal* 40 (2002) 492–515.
- [9] P. Benner, S. Gugercin, K. Wilcox, A survey of projection-based model reduction methods for parametric dynamical systems, *SIAM Review* 57 (2015) 483–531.
- [10] M. L. Adams, Subcell balance methods for radiative transfer on arbitrary grids, *Transport Theory and Statistical Physics* 26 (1997) 385–431.
- [11] S. Volkwein, Model reduction using proper orthogonal decomposition, lecture Notes, University of Konstanz (2013).
- [12] V. Ya. Gol'din, A quasi-diffusion method of solving the kinetic equation, *USSR Comp. Math. and Math. Phys.* 4 (1964) 136–149.
- [13] V. Ya. Gol'din, B. N. Chetverushkin, Methods of solving one-dimensional problems of radiation gas dynamics, *USSR Comp. Math. and Math. Phys.* 12 (1972) 177–189.
- [14] V. Ya. Gol'din, D. A. Gol'dina, A. V. Kolpakov, A. V. Shil'kov, Mathematical modeling of hydrodynamics processes with high-energy density radiation, *Problems of Atomic Sci. & Eng.: Methods and Codes for Numerical Solution of Math. Physics Problems* 2 (1986) 59–88, in Russian.
- [15] L. H. Auer, D. Mihalas, On the use of variable Eddington factors in non-LTE stellar atmospheres computations, *Monthly Notices of the Royal Astronomical Society* 149 (1970) 65–74.
- [16] D. Y. Anistratov, Stability analysis of a multilevel quasidiffusion method for thermal radiative transfer problems, *Journal of Computational Physics* 376 (2019) 186–209.
- [17] J. A. Fleck, J. D. Cummings, An implicit monte carlo scheme for calculating time and frequency dependent nonlinear radiation transport, *Journal of Computational Physics* 8 (1971) 313–342.
- [18] C. W. Rowley, J. E. Marsden, Reconstruction equations and the karhunen-loève expansion for systems with symmetry, *Physica D* 142 (2000) 1–19.
- [19] J. Reiss, P. Schulze, J. Sesterhenn and V. Mehrmann, The shifted proper orthogonal decomposition: A mode decomposition for multiple transport phenomena, *SIAM Journal of Scientific Computing* 40 (2018) A1322–A1344.
- [20] G. L. Olson, L. H. Auer and M. L. Hall, Diffusion, P_1 , and other approximate forms of radiation transport, *Journal of Quantitative Spectroscopy & Radiative Transfer* 64 (2000) 619–634.